Bilge International Journal of Science and Technology Research

ISSN: 2651-401X
e-ISSN: 2651-4028
Research Article / Araştırma Makalesi
2021, Volume: 5, Issue: 2, 91-100
Received: 20.02.2021; Accepted: 03.06.2021
DOI: 10.30516/bilgesci.883935

Monitoring of Deep-Seated Landslides at Karaoğlan Catchment Using Radar Interferometry Techniques (Mersin, Turkey)

Muhterem Küçükönder[1]*, Tolga Çan[2]

Abstract: Landslide inventory mapping studies around Mersin and Erdemli regions of southern Turkey revealed that numerous old large-scale and recent small-scale landslides were presumably aroused in different time intervals. While the recent active landslides have been mostly triggered by excessive rainfall, old landslides are considered to be occurred by geomorphologic valley incision processes besides the other preparatory environmental conditions. The evaluation of the spatial distribution of old landslides present retrogressive, deep-seated with complex and rotational slides in the ophiolites and ophiolitic melange units comprising also overlying reefal limestones. In this study, surface deformations caused by landslides were evaluated using radar interferometry techniques for a specified period in Karaoğlan catchment. Landslide related deformations were detected over radar images of L-band ALOS-PALSAR sensor for the years between 2007 and 2011. Active landslides are investigated in detailed cross-sections. The mean displacement from differential interferogram cross-sections was measured 3.5 cm in the LOS direction. Differential SAR interferometry for the studied period depicts that the average rate of movement for the entire area is prolonged with a rate of 10 mm/yr.

Keywords: Landslide, SAR interferometry, DinSAR, Mersin

[1]**Address:** Kahramanmaras Sutcu Imam University, Faculty of Science and Letters, 46050, Kahramanmaras/Turkey
[2]**Address:** Cukurova University, Faculty of Engineering, 01330, Adana/Turkey

***Corresponding author**: mhtrm.kckndr@gmail.com

Citation: Küçükönder, M., Çan, T. (2021). Monitoring of Deep-Seated Landslides at Karaoğlan Catchment Using Radar Interferometry Techniques (Mersin, Turkey). Bilge International Journal of Science and Technology Research, 5(2): 91-100.

1. INTRODUCTION

Landslides are among the most important and common geomorphic processes that produce systematic changes in the development and evolution of landforms. Each type of landslide, i.e. flow, fall, topple, slide, produces a distinct morphological imprint on the landform under similar geo-environmental conditions (Cruden and Varnes 1996). Landslide inventories and their spatial and temporal variations in conjunction with the preparatory and triggering factors are essential for the landslide susceptibility and hazard assessments. The rate of movement and monitoring of landslides are also important during the landslide risk evaluation and management studies.

Ground-based instrumental monitoring of landslides in mountainous terrains for a long period is a rather difficult mission. The development of remote sensing techniques utilizing both optic and radar imaging has compensated for some of the difficulties, such as time-consuming. Landslide mapping and monitoring will continue to remain complex and challenging even with ground monitoring techniques. It is clear that InSAR techniques (differential, SBAS and CTM/ PSInSAR) are making significant addition in monitoring seasonal slope activity at high-risk sites (Singhroy 2008). The greater availability and improved capability of radar sensors and the development of more advanced data processing techniques increasingly enabled the use of SAR data in ground deformations (Massonnet and Feigl 1998; Rosen et al. 2000; Metternicht et al. 2005; Catani et al. 2005; Colesanti and Wasowski 2006; Rott and Nagler 2006; Zhou et al. 2009; Hastaoğlu et al. 2018).

Differential Synthetic Aperture Radar interferometry (DInSAR), which considers the phase differences of SAR acquisitions of the area under illumination at different time intervals, is one of the widely used technique for introducing ground deformations on a regional scale (Ferretti et al. 2000; Hanssen 2001; Catani et al. 2005; Rott

and Nagler 2006). There are many case studies related to landslide movements using DInSAR techniques in the international literature (e.g. Kimura and Yamaguchi 2000; Berardino et al. 2003; Farina et al. 2004; Strozzi et al. 2005; Colesanti and Wasowski 2006; Singhroy et al. 2008; Delacourt et al. 2009; Guzzetti et al. 2009; Strozzi et al. 2010; Delgado et al. 2011; Singhroy et al. 2011; Bovenga et al. 2012; Calo et al. 2012). Meanwhile, there are some cumbersome situations either derived from geo-environmental setting itself (land cover, topography and landslide characteristics etc.) or SAR system parameters (wavelength, temporal and normal baselines etc.) in addition to data processing techniques (Metternicht et al. 2005; Colesanti and Wasowski 2006; Rott 2009; Cascini et al. 2010).

DInSAR studies dealing with landslides are generally focused on single landslide (Refice et al., 2001). The present study attempts to investigate landslide related surface deformations in catchment scale using the DInSAR technique. The study area, Karaoglan catchment of 52.8 km^2, is located in the southern front of the Bolkar Mountains. At first, land cover, geological, and geomorphic settings of the catchment was summarized with a particular relationship on landslide occurrences. Then landslide inventory map of the study area was presented. Finally, landslide related surface deformations were interpreted.

1.1. Settings of the area

The study area is one of the sub-basin located in the Gilindirez catchment on the southern flanks of the Bolkar Mountain range in the Eastern Mediterranean, which is dissected by the numerous NW-SE trending sub-parallel rivers that drained to the Mediterranean (Figure 1). Typical Mediterranean climate prevails in the area with hot, dry summers and mild, wet winters. The average temperatures vary between 25-33° in summer and 9-15° in winter. The mean annual rainfall is about 600 mm and the majority of the rainfall amount is recorded between December to February. However, extreme daily rainfalls of 199.5 mm and 175.4 mm were experienced on 26 December 1968 and 03 December 2001, respectively.

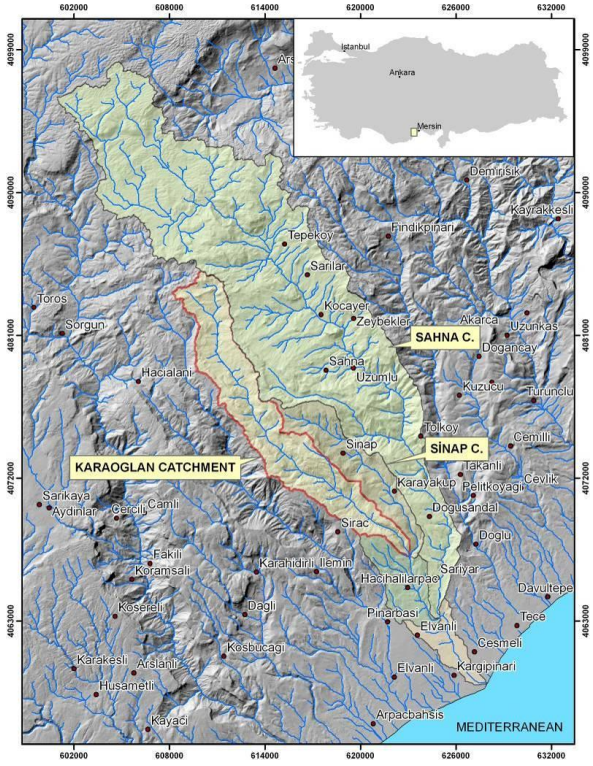

Figure 1. Location map of the study area

Land cover map, produced by using ALOS AVNIR image of 10 m resolution, acquainted on May 2007, revealed that bare land and rock knobs represent 20 % of the study area while the 38 % of the area corresponds with dense to sparse forest cover (Figure 2). There is no rural settlement within the study area, so apart from 7 % of Orchards area almost no anthropic landscape change prevails.

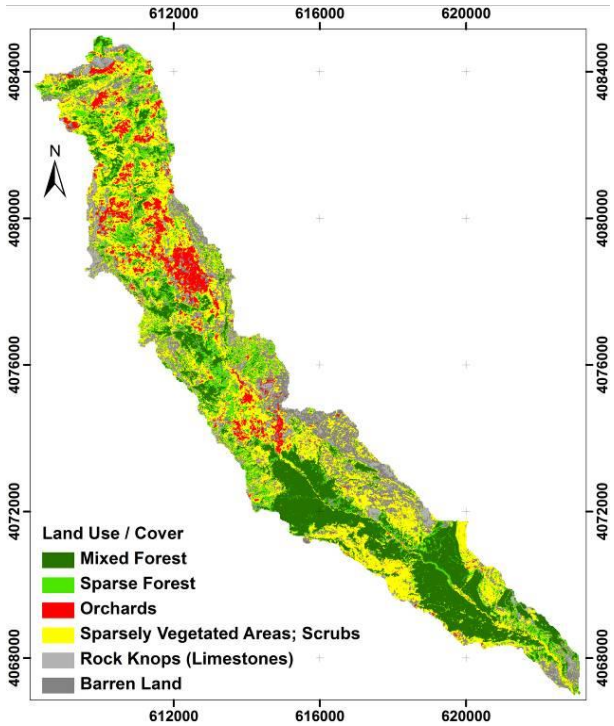

Figure 2. Land use/cover map of the Karaoglan catchment.

The geologic setting of the area can be classified into two main features. Tertiary units of the Neogene Adana Basin (Yetiş 1988) represent the cover units, whereas the

basement rocks are characterized by remnants of oceanic lithosphere so-called "Mersin Ophiolite Complex" (Pampal 1987) (Figure 3).

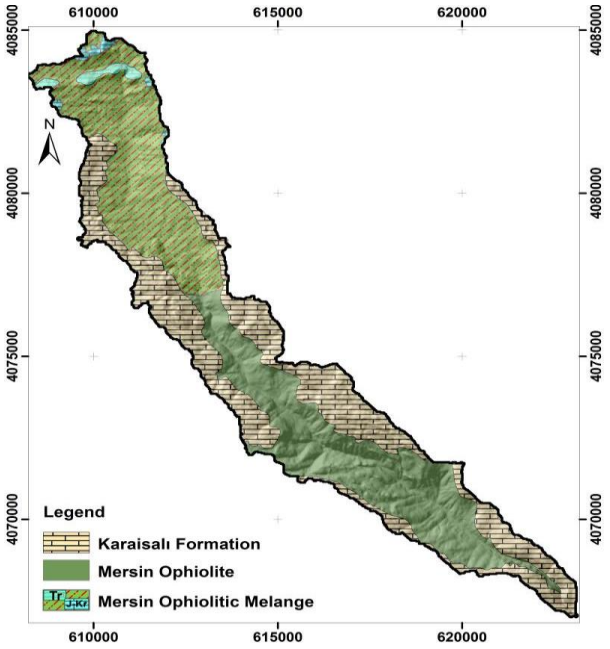

Figure 3. Geological map of the study area (Modified after Pampal (1987)).

The Mersin ophiolite complex, with almost 6 km of thickness, consists of (in ascending structural order): ophiolitic melange, subophiolitic metamorphics, mantle tectonites, ultramafic and mafic cumulates, alkaline-tholeiitic basaltic volcanic in association with deep marine sediments (Parlak et al. 1996). In the study area, ophiolitic melange and tectonites constitute the basements units, which unconformably overlain by Miocene reefal carbonates (Figure 4). Parlak and Robertson (2004) identified four lithological associations within the Mersin Ophiolitic Melange which are (1) the Upper Permian–Upper Cretaceous shallow-water carbonate association; (2) the Upper Triassic–Upper Cretaceous volcanic–terrigenous–pelagic association; (3) the Upper Jurassic–Upper Cretaceous basalt–radiolarite pelagic limestone association and (4) the Upper Cretaceous ophiolite-derived association. Each of these lithological associations varies from broken formation to melange and is associated with a matrix of both sedimentary and tectonic origin (Parlak and Robertson 2004). The Melange unit is structurally overlain by the Mersin Ophiolite. In the study area, the Mersin Ophiolite is represented by mantle tectonites mainly comprising serpentinized harzburgite and dunits (Figure 5 a and b). Surface and subsurface karstic landforms are characteristics on the reefal carbonate sequence (Figure 5 c and d).

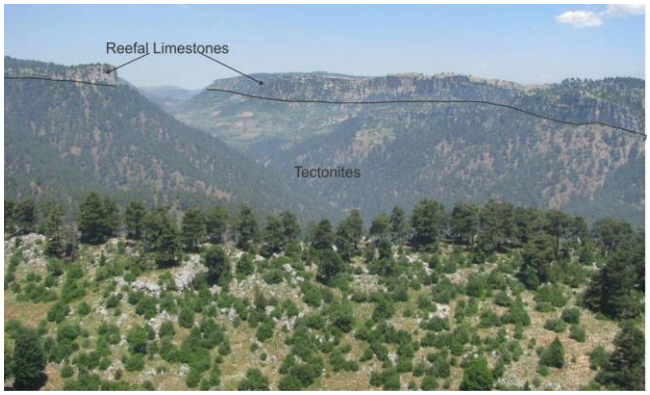

Figure 4. The contact relationship between Reefal limestones (Karaisali formation) and tectonites of the Mersin Ophiolite.

Figure 5. Close views from the serpantinized harzburgites (a and b). Note that degree of serpantinization is higher in (b). Surface karstic features (c) and old underground karstic river system (d) observed in reefal limestones.

In the Karaoglan sub-catchment, elevation ranges from 250 m to 1830 m. The area with an altitude higher than 1000 m is about 75 % of the entire catchment (Figure 6a). The valley sides are steep and V-shaped. Steep slopes higher than 40 degrees mostly correspond to either limestone outcrops along the ridges or river flanks along the bottom of the valley (Figure 6b). The majority of the slope aspects are in SW and NE directions (Figure 6c). The length of the catchment is about 26 km with an average width of 2.5 km. The morphometric analysis results with a circulation ratio of 0.118, shape factor of 12.91 and form factor 0.077; it is a highly elongated catchment with high relief.

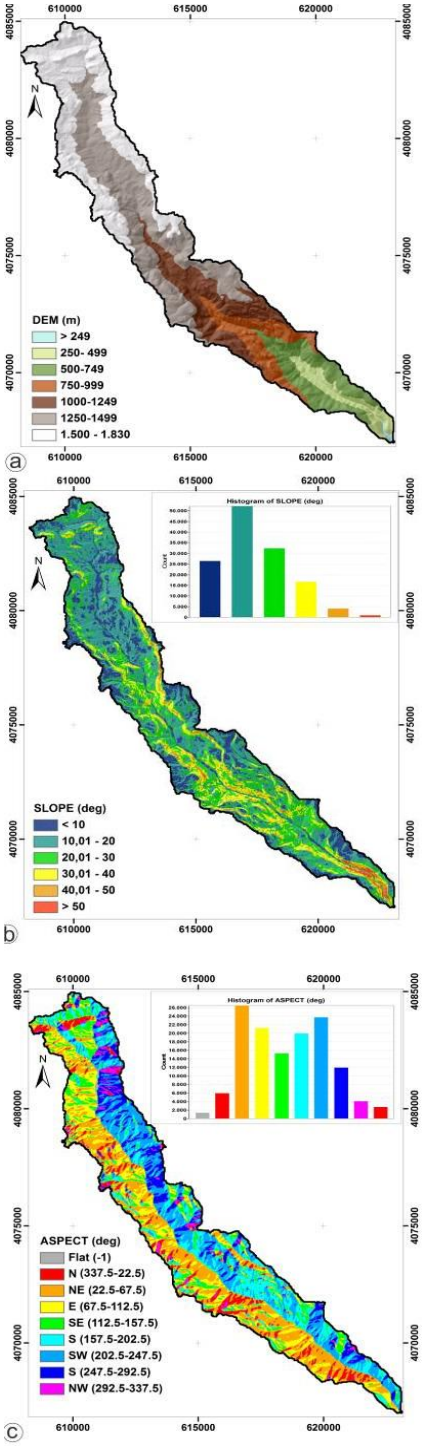

Figure 6. DEM (a), slope (b) and aspect (c) maps of the study area.

The stages of landscape evolution and an indication of erosion status of the Karaoglan and adjacent sub-catchments were evaluated by hypsometric analysis. The hypsometric curve is related to the volume of the soil mass in the catchments and the amount of erosion that had occurred in a basin against the remaining mass (Hurtrez et al. 1999). It is a continuous function of the non-dimensional distribution of relative basin elevations with the relative area of the drainage basin (Strahler 1952). The hypsometric integral (HI) is a geomorphological parameter classified under the geologic stages of catchment development. It assumes importance in the estimation of erosion status of catchment and subsequent prioritization for taking up soil and water conservation activities. The hypsometric curves with HI values were given in Figure 7. As seen from Figure 7, the concave upward hypsometric curve of the Karaoglan sub-catchment indicates in equilibrium stage of erosion while the others are relatively in the mature stage. The HI value of 64.1 % for the Karaoglan sub-catchment refers that only 36 % of the present volume has been carried away due to hydrologic processes and land degradation factors.

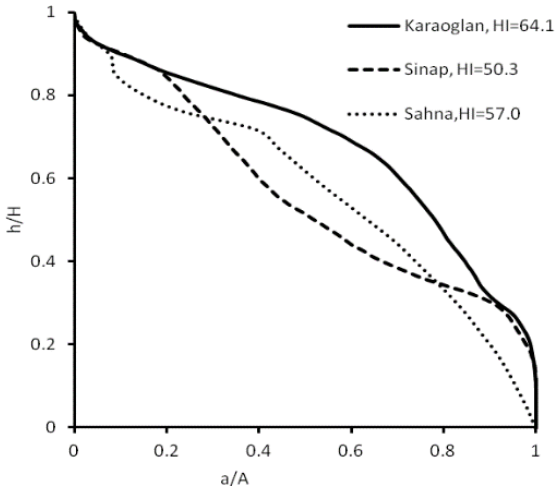

Figure 7. Hypsometric curves of the sub-catchments in the Gilindirez catchment.

2. MATERIAL AND METHOD

2.1. Landslide inventory

The landslide inventory map of the study area was prepared after three available aerial photographs dated 1969, 1990 and 2001. The latter set is 1:10,000 scale colored infrared while the others are panchromatic in 1:15,000 scale. Forty-three landslides covering 11.97 km^2 were identified, ranging from 2440 m^2 to 2.45 km^2 (Çan et al. 2009) (Figure 8a). The landslide affected area corresponds to almost 23 % of the Karaoglan catchment. Most of the landslides are complex deep-seated. Some of the tension cracks observed outside the present catchment boundary and successive limestone blocks within the slide masses from the valley bottom towards the ridges support the ongoing retrogressive movement of the landslides (Figure 8b). Tension cracks generally observed along with the two main discontinuity sets with general strikes of N60W and N30E.

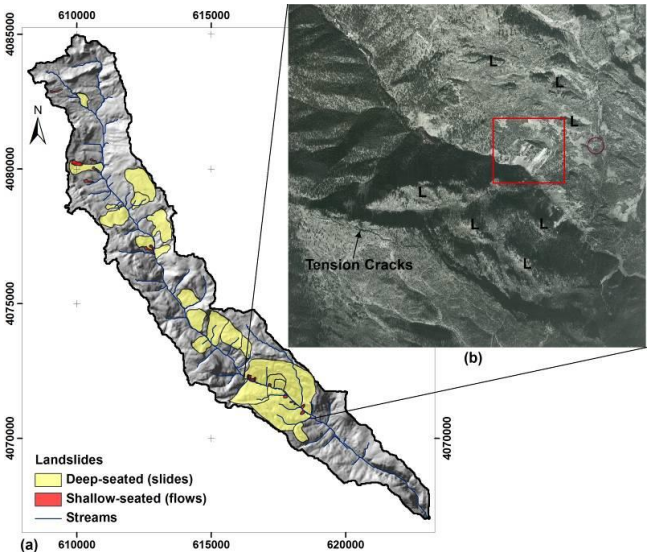

Figure 8. Landslide inventory map of the Karaoglan catchment (a) and aerial photograph taken in 1969 that depicts the largest deep-seated landslides and major tension cracks (b), L indicates some of the successive limestone blocks which align perpendicularly to the main direction of movements (Çan et al. 2009).

The main landslide movement types are rotational slides (Figure 9a), but along the crown of the landslides rockfall events observed on almost vertical hill slopes made up of reefal carbonates (Figure 9b). Tension cracks, ranging from several tens of meters to more than 1 km in length, were observed behind the main scarps in places indicating retrogressive character considering their distribution of activity (Figure 9c and d).

Shallow seated landslides were only identified on aerial photographs dated 1969, triggered by excessive rainfall (700 mm/month) in December 1968. Otherwise, the ongoing landslide activities were primarily observed in the existing slide masses as secondary movements (Figure 10). They are good pieces of evidence for the actual geomorphic dynamics in the development of the region's landforms. Landslides located towards the downstream part of catchments are relatively active due to higher river and valley side slope gradients. Depleted masses along the valley bottom present a high slope gradient due to the river incision and erosion processes. Consequently, earth and debris flow along the valley bottom are also common in highly serpentinized ultramafic rocks.

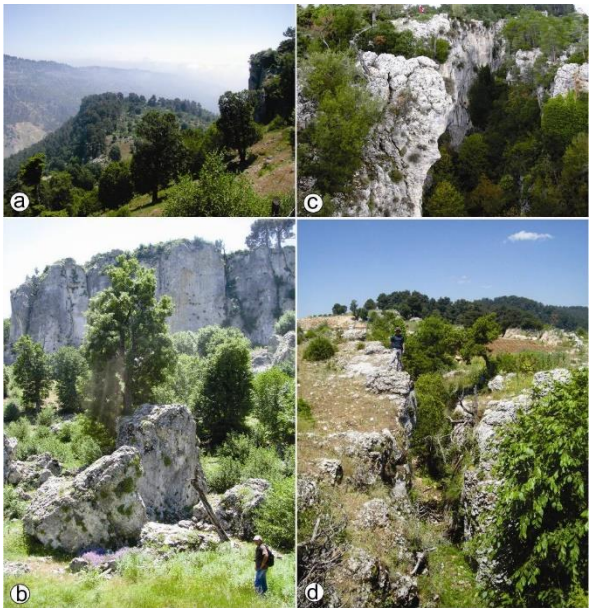

Figure 9. Components of complex deep-seated landslides on NE slope. Rotational slide (a), rockfall events (b), and tension cracks behind the main scarps (c and d).

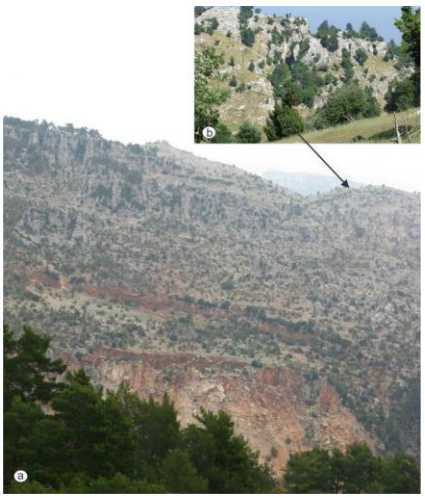

Figure 10. Secondary retrogressive landslide generation within the old slide mass (a) and tension cracks on the upper bound of the landslide (b).

2.2. INSAR Data

Significant challenges prevail regarding the practical applicability of satellite radar data to landslide investigations (Colesanti and Wasowski 2006; Calo et al. 2012). Coherence, a prerequisite for the processing interferogram, compares the correlation between the two SAR images. Coherence loss is the main factor, including several components that affects the quality and accuracy of the results. The loss of coherence (decorrelation) can be affected by terrain morphology, land cover, rate of movements, temporal baseline, normal baseline and other technical details during the interferogram generation (Singhroy 2008).

The wavelength also has a considerable role in the SAR systems. Strozzi et al. (2005) and Sandwell et al. (2008) also mentioned that L-band interferometry could complement the existing applications based on C-band because of its capacity to penetrate the vegetation canopy,

and thus, achieve high coherence interferograms over vegetated areas. Furthermore, the larger wavelength is more appropriate for rapid mapping displacements. The use of larger wavelength avoids problems related to the phase measurements' intrinsic ambiguity (Strozzi et al. 2005).

In this study, PALSAR (Phased Array L-band Synthetic Aperture Radar) sensor has been preferred due to its advantages that are briefly mentioned above. PALSAR images have 236 mm wavelength, 10 m (FBS) and 20 m (FBD) spatial resolutions, high critical baselines (14 km for FBS and 7.4 km for FBD) and 34.3 degrees of look angle. The revisiting time of the sensor is 46 days. Despite its 46 days revisiting time, only 16 archive images were acquired for the area under interest. Considering the preferred baseline, only five images of ascending mode could be available for interferogram generation from 17 September 2007 to 10 February 2011 of the study area. The interferometric data sets, in addition to the normal and temporal baselines, are summarized in Table 1. The interferometric pair for 19 June 2008 - 22 June 2009 has the most significant baseline for both temporally and perpendicularly.

Table 1. Baselines of the interferometric pairs.

	Temporal Baseline (day)	Perpendicular Baseline (m)
17Sep.2007 - 19June2008	270	524
19June2008 - 22June2009	368	718
26Dec.2010 - 10Feb.2011	-46	-670

2.3. Analysis

The PALSAR Level 1.1 data were processed to Single-Look Complex (SLC) images. All DinSAR process was carried out with Sarscape 5.1. The baseline was first estimated from the orbit data and subsequently refined based on the fringe rate in range and azimuth directions. Interferometric processing was done to 5 azimuths and one range looks with common-band filtering after co-registration of the SLC images. The topographic flattening was estimated from 20x20m Digital Elevation Models (DEM) derived from a 1:25,000 scale digital topographic map with a contour interval of 10 m. The next step of the DInSAR processing was followed by adaptive phase filtering and coherence estimation, which are important to improve the accuracy of surface deformations. Phase unwrapping was performed after adaptive filtering with the Goldstein method, applying a minimum cost flow algorithm. A coherence threshold of 0.17 was used to reduce the unwrapping errors. Finally, the unwrapped interferograms were converted to displacements expressed in meters along the line-of-sight direction of the satellite before geocoding.

3. RESULTS

The obtained displacement rates generally coincide with the landslides located especially on the slopes with dip directions towards SW. The mean displacements for the first (Figure 11a), second (Figure 11b) and third (Figure 11c) pairs are -0.0326 m, -0.046 m and -0.026 m, respectively. Comparing the first and second FBD pairs shows that the loss of coherence is gradually higher with increasing temporal baseline. Although the acquisition for the second pairs is the same, the highest loss of coherence with 5 % was observed due to the highest perpendicular baseline. The better performance for the landslide affected areas in Figure 11c is considered for the shortest temporal baseline of 46 days with 10 m of spatial resolution in FBS mode.

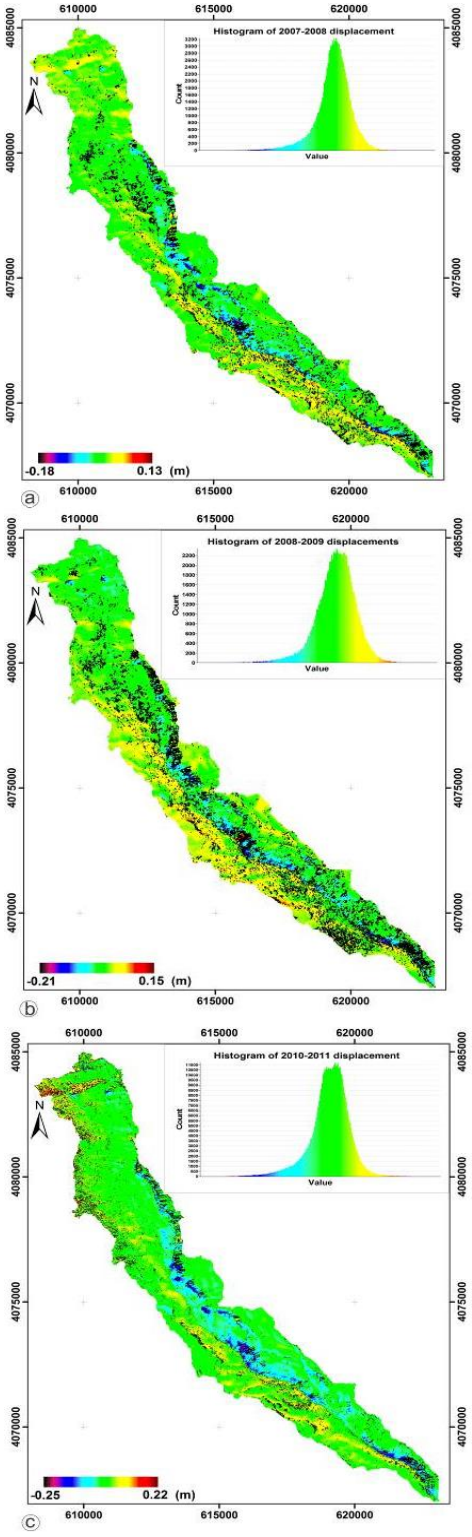

Figure 11. Geocoded displacement maps in the line-of-sight direction for the periods 2007 - 2008 (a), 2008 - 2009 (b) and 2010 - 2011 (c). The histograms of ground deformations are also shown for each map.

The coherence losses related to land use and morphology were generally observed in orchards and steep slopes of serpentinized harzburgites. When the terrain slope is close to the radar off-nadir angle, the cell dimension becomes very large and all the details are lost. Moreover, when the terrain slope exceeds the radar off-nadir angle, the scatterers are imaged in reverse order and superimposed on the contribution coming from other areas. This effect is called layover. On the other hand, when the terrain slope decreases to the flat horizontal reference surface, the resolution cell dimension decreases. The minimum resolution cell dimension (i.e. equal to the slant range resolution) is reached when the terrain is parallel to the LOS. This is also the lower slope limit that can be imaged at all by a SAR system since, beyond this angle, the terrain is in shadow (Hanssen 2001; Ferretti et al. 2007). In order to consider the restriction due to layover and shadow effects, the general incidence angle was recalculated with respect to the local incidence angles of each pixel. Almost 3.5 % of total layover and shadow effects were calculated in the study area (Figure 12). The area affected by layover effects mostly corresponds to SW oriented steep slopes of reefal carbonates, whereas the shadow effects, which are much less than layover effects, are sparsely distributed on slopes facing to the NE, in general.

Surface deformations and their relationship between landslides were compared by three profiles. The first landslide presents typical rotational failure and comprises units of reefal limestone underlying tectonites. The movement rates were mostly observed on the head of the landslide and the maximum displacement up to 0.15 m was identified on the 2010-2011 pair (Figure 13). On the main scarp, secondary movements such as rockfall caused some decorrelation. The tension cracks along the crown suggest that the distribution of activity of the landslide has a retrogressive character (Figure 14). In the accumulation zone, secondary rotational movements were also observed in situ. So apart from the head of the landslide, no distinct movement was noticed along the main landslide body.

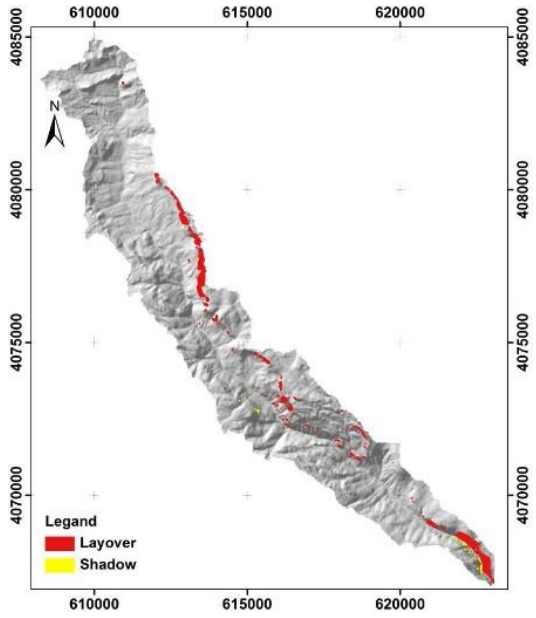

Figure 12. Spatial distribution of the layover and shadow affected pixels in the study area.

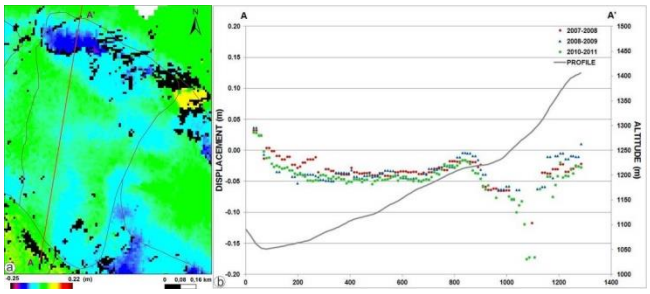

Figure 13. Measurement rates in the PALSAR line-of-sight direction of corresponding pixels in the cross-section of A-A'.

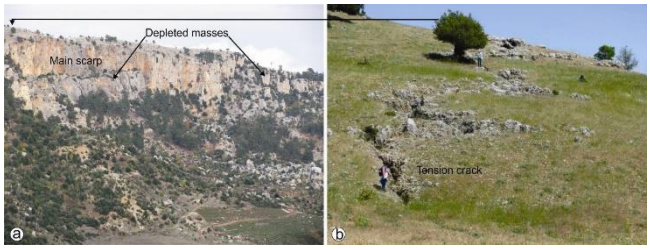

Figure 14. A general view for the rotational landslide for section A-A' (a) and the status of tension crack on the crown (b). The reference tree in Figure (b) is given for the location of the tension crack in Figure (a).

The second site is characterized by the largest landslide of the study area (Figure 15a). The total surface area of the landslide is 2.2 km^2. The elevation range between the valley bottom and the topographic divide is 550 m. At least six movements with retrogressive character were identified in the main landslide body considering the successive old landslide scarps and subparallel strings of the reefal carbonate knobs extending perpendicularly to the direction of the movement. In addition to this, new reactivations observed along the toe of the landslide indicate that new retrogressive rotational slides are in progress as a second phase in the depleted landslide mass (see Figure 10). The displacement fluctuations along the profile in Figure 15b correspond to secondary scarps in the slide mass. The largest displacements were observed along the toe of the landslide, where secondary retrogressive movements initiated. On the opposite valley side, another large-scale landslide is also located. By contrast to the second profile, no significant movement was observed along the toe of this landslide except some earth flows. Meanwhile, the retrogressive character in the whole depleted mass is identical. In some places behind the crown, tension cracks up to several tens of meters are located. According to the morphologic features on the mass, the observed activity of the landslide seems less active than the opposite side. The displacement profile given in Figure 15c supports the field observations and almost no significant deformation was measured.

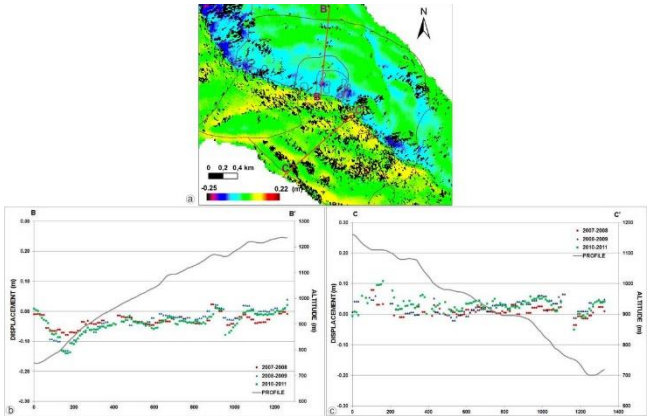

Figure 15. Measurement rates in the PALSAR line-of-sight direction of corresponding pixels along the B-B' and C-C' cross sections.

Despite the tension cracks observed behind the crown together within the depleted mass, which represent different stages of landslide activity, the small amount of displacement obtained during the investigated time period suggest that the landslides in the study area are in a dormant state of activity. However, visual analyses of aerial photographs taken in 1969 and 2001 clearly show the ongoing ground deformations (Figure 16). JERS and PALSAR are the only L-Band imaging radar sensors and both of them are completed their missions. The active operational time interval for the JERS and PALSAR was 1992-1998 and 2006-2011, respectively. In order to observe surface deformations in such extremely slow-moving landslide areas, radar sensors of longer operational time duration and more frequent data acquisitions should be provided. It is hoped that the next generations L-band sensors will compensate for some of the technical limitations in the near future.

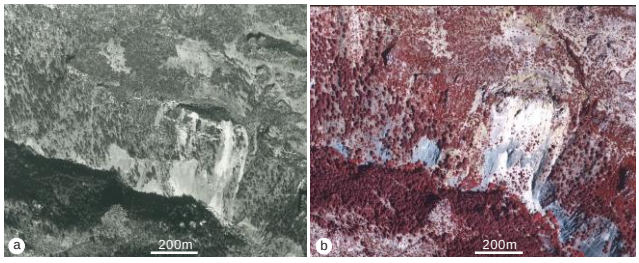

Figure 16. Aerial photographs were taken in 1969 (a) and 2001 (b). The ground deformation, especially on the head and depletion zone, is identical.

4. DISCUSSION AND CONCLUSIONS

Southern flanks of the Bolkar Mountain range dissected by numerous river systems which generally extend NW to SE direction and discharge into the Mediterranean have been severely affected by deep-seated landslides of various degree of activity. In this paper, surface deformations caused by landslides were analyzed using L-Band ALOS PALSAR images during 2007-2011, in a 52.8 km^2 size Karaoglan catchment, which conforms to general characteristics of the region. It has seen that 23 % of the area has mostly affected by large scale deep-seated landslides. Long tension cracks behind the crowns of some of the landslides, even extending outside the present topographic divide, indicate their retrogressive distribution of activity.

The application of the DInSAR technique to the Karaoğlan catchment suggests that no significant reactivation of landslides were observed during the period under investigation. However, small displacements that characterised the mechanisms within the different part of the landslides were observed. The mean rate of displacement and velocity from differential interferograms for the study area between 2007-2011 is 3.5 cm and 10 mm/yr, respectively. Although the spatial extent of the study area with respect to the LOS and the rate and direction of movements of landslides are convenient for DInSAR applications, the main drawbacks of this study are the limited number of available interferometric data and the absence of ground-based verifications.

If sufficient data are available for more extensive time spans, the DInSAR technique using L-Band missions could play a significant role in monitoring displacements of landslides on a regional scale, also providing an alternative and/or complementary to the ground-based monitoring systems.

After 2000, various active remote sensing systems with different resolution features are operational. Among these, new generation active sensors such as X-band TerraSAR-X, L-band ALOS-2 could not be used in this study due to their cost. Free of charge Sentinel 1 active series images and techniques such as persistent scatterer interferometry (PSInSAR) or Small Baseline Interferometry (SBAS) are planned to be used in future studies.

ACKNOWLEDGEMENTS

Landslide inventory data used in this study was prepared as part of the project (TUBITAK CAYDAG 107Y138) supported by the Scientific and Technical Research Council of Turkey (TUBITAK). This work was also supported by the Scientific Research Project Fund of Çukurova Üniversitesi under project number MMF2011BAP21.

REFERENCES

Berardino, P., Costantini, G., Franceschetti, G., Iodice, L., Pietranera, L., Rizzo, V., (2003). Use of differential SAR interferometry in monitoring and modelling large slope instability at Matera (Basilicata, Italy). Engineering Geology, 68, 31-51.

Bovenga, F., Wasowski, J., Nitti, D.O., Nutricato, R., Chiaradia, M.T., (2012). Using COSMO/SkyMed X-band and ENVISAT C-band SAR interferometry for landslides analysis. Remote Sensing of Environment, 119, 272-285.

Calo, F., Calcaterra, D., Iodice, A., Parise, M., Ramondini, M., (2012). Assessing the activity of a large landslide in southern Italy by ground-monitoring and SAR interferometric techniques. International Journal of Remote Sensing, 33, 3512-3530.

Cascini, L., Fornaro, G., Peduto, D., (2010). Advanced low- and full-resolution DInSAR map generation for slow-moving landslide analysis at different scales. Engineering Geology, 112, 29-42.

Catani, F., Farina, P., Moretti, S., Nico, G., Strozzi, T., (2005). On the application of SAR interferometry to geomorphological studies: estimation of landforms attributes and mass movements. Geomorphology, 66, 119-131.

Colesanti, C., Wasowski, J., (2006). Investigating landslides with space-borne Synthetic Aperture Radar (SAR) interferometry. Engineering Geology, 88, 173-199.

Cruden, D.M., Varnes, D.J., (1996). Landslide types and processes. In: Turner AK, Schuster LR (ed) Special Report 247: Landslides: Investigation and Mitigation, Transportation Research Board, Washington, pp 129-177.

Çan, T., Duman, T.Y., Çil, E., Mazman, T., (2009). GIS Based Landslide Inventory, Susceptibility, Hazard and Risk Assessment of the Northern Parts of Mersin Central and Erdemli Districts (In Turkish). TÜBİTAK-ÇAYDAG Project no: 107Y138.

Delacourt, C., Raucoules, D., Le Mouélic, S., Carnec, C., Feurer, D., Allemand, P., Cruchet, M., (2009). Observation of a large landslide on la reunion island using differential SAR interferometry (JERS and Radarsat) and correlation of optical (Spot5 and Aerial) images. Sensors, 9, 616-630.

Delgado, J., Vicente, F., García-Tortosa, F., Alfaro, P., Estévez, A., Lopez-Sanchez, J.M., Tomas, R., Mallorquí, J.J., (2011). A deep seated compound rotational rock slide and rock spread in SE Spain: Structural control and DInSAR monitoring. Geomorphology, 129, 252-262.

Farina, P., Colombo, D., Fumagalli, A., Marks, F., Moretti, S., (2006). Permanent Scatterers for landslide investigations: Outcomes from the ESA-SLAM project. Engineering Geology, 88, 200-217.

Ferretti, A., Prati, C., Rocca, F., (2000). Nonlinear subsidence rate estimation using permanent scatterers in differential SAR interferometry. IEEE Geoscience and Remote Sensing Letters, 38, 2202-2212.

Ferretti, A., Massonnet, D., Monti Guarnieri, A., Prati, C., Rocca, F., (2007). InSAR Principles: Guidelines for SAR Interferometry Processing and Interpretation. ESA Publications TM-19 http://www.esa.int/About_Us/ESA_Publications/InSAR_Principles_Guidelines_for_SAR_Interferometry_Processing_and_Interpretation_br_ESA_TM-19. Accessed 16 June 2013.

Guzzetti, F., Manunta, M., Ardizzone, F., Pepe, A., Cardinali, M., Zeni, G., Reichenbach, P., Lanari, R., (2009). Analysis of ground deformation detected using the SBAS-DInSAR technique in Umbria, Central Italy. Pure and Applied Geophysics, 166, 1425-1459.

Hanssen, R., (2001). Radar Interferometry: Data Interpretation and Error Analysis. Kluwer Academic Publishers, Dordrecht.

Hastaoglu, K.O., Poyraz, F., Turk, T., Yılmaz, I., Kocbulut, F., Demirel, M., Sanli, U., Duman, H., Balik Sanli, F., (2018). Investigation of the success of monitoring slow motionlandslides using Persistent Scatterer Interferometry and GNSS methods, Survey Review, 50 (363), 475-486.

Hurtrez, J., Lucazeau, F., Lave, J., Avouac, J., (1999). Investigation of the relationships between basin morphology, tectonic uplift, and denudation from the study of an active fold belt in the Siwalik Hills, Central Nepal. Journal of Geophysical Research, 104, 12779-12796.

Kimura, H., Yamaguchi, Y., (2000). Detection of landslide areas using radar interferometry. Photogrammetric Engineering and Remote Sensing, 66, 337-344.

Massonnet, D., Feigl, K.L., (1998). Radar interferometry and its application to changes in the earth's surface. Reviews of Geophysics, 36, 441-500.

Metternicht, G., Hurni, L., Gogu, R., (2005). Remote sensing of landslides: an analysis of the potential contribution to geo-spatial systems for hazards assessment in mountainous environments. Remote Sensing of Environment, 98, 284-303.

Pampal, S., (1987). Geology of the Guzeloluk-Sorgun (Mersin) region (In Turkish). Journal Of The Faculty Of Engineering And Architecture Of Gazi University, 2, 143-170.

Parlak, O., Delaloye, M., Bingöl, E., (1996). Mineral chemistry of ultramafic-mafic cumulates as an indicator of the arc-related origin of the Mersin ophiolite (southern Turkey). Geologische Rundschau, 85, 647-661.

Parlak, O., Robertson, A.H.F., (2004). The ophiolite-related Mersin Melange, southern Turkey: Its role in the tectonic-sedimentary setting of the Tethys in the eastern Mediterranean region. Geological Magazine, 141, 257-286.

Refice, A., Bovenga, F., Guerriero, L., & Wasowski, J. (2001). DInSAR applications to landslide studies. In IGARSS 2001. Scanning the Present and Resolving the Future. Proceedings. IEEE 2001 International Geoscience and Remote Sensing Symposium (Cat. No. 01CH37217) (Vol. 1, pp. 144-146). IEEE.

Rosen, P., Hensley, S., Joughin, I., Li, F., Madsen, S., Rodriguez, E., Goldstein, R., (2000). Synthetic aperture radar interferometry. Proceedings of the IEEE, 88 (2000), 333-382.

Rott, H., Nagler, T., (2006). The contribution of radar interferometry to the assessment of landslide hazards. Advances in Space Research, 37, 710-719.

Rott, H., (2009). Advances in interferometric synthetic aperture radar (InSAR) in earth system science. Progress in Physical Geography, 6, 769-791.

Sandwell, D., Myer, D., Mellors, R., Shimada, M., Brooks, B., Foster, J., (2008). Accuracy and resolution of ALOS interferometry: Vector deformation maps of the Father's day intrusion at Kilauea. IEEE Transactions on Geoscience and Remote Sensing, 46, 3524-3534

Singhroy, V., Alasset, P.J., Couture, R., Froese, C., (2008). InSAR monitoring of landslides in Canada. Proceedings of the IEEE International Geoscience and Remote Sensing Symposium (IGARSS'08), 3, 202-205.

Singhroy, V., (2008). Satellite remote sensing applications for landslide detection and monitoring. In: Sassa, K., Canuti, P., (ed) Landslide Disaster Risk Reduction, Springer, Berlin, pp 143-158.

Singhroy, V., Li, J., Charbonneau, F., Pavlic, G., Segin, G., (2011). InSAR Monitoring of Landslides affecting strategic Transportation Corridors. Proceedings 34th International Symposium on Remote Sensing of Environment, Sydney. 3p.

Strahler, A.N., (1952). Hypsometric (area-altitude) analysis of erosional topology. Geological Society of America Bulletin, 63, 1117-1142.

Strozzi, T., Farina, P., Corsini, A., Ambrosi, C., Thuring, M., Zilger, J., Wiesmann, A., Wegmüller, U., Werner, C., (2005). Survey and monitoring of landslide displacements by means of L-band satellite SAR interferometry. Landslides, 2, 193-201.

Strozzi, T., Delaloye, A., Kääb, A., Ambrosi, C., Perruchoud, E., Wegmüller, U., (2010). Combined observations of rock mass movements using satellite SAR interferometry, differential GPS, airborne digital photogrammetry and airborne photography interpretation. Journal of Geophysical Research, 115(F1), F01014

Yetiş, C., (1988). Reorganization of the Tertiary Stratigraphy in the Adana Basin, Southern Turkey. Newsletters on Stratigraphy, 20, 43-58.

Zhou, X., Chang, N., Li, S., (2009)s. Application of SAR Interferometry in earth and environmental science research. Sensors, 9, 1876-1912.